



Cite this: *Chem. Sci.*, 2025, **16**, 22481

All publication charges for this article have been paid for by the Royal Society of Chemistry

## Multi-technique characterization of rhodium gem-dicarbonyls on $\text{TiO}_2(110)$

Moritz Eder, <sup>\*a</sup> Faith J. Lewis, <sup>a</sup> Johanna I. Hütner, <sup>a</sup> Panukorn Sombut, <sup>a</sup> Maosheng Hao, <sup>b</sup> David Rath, <sup>a</sup> Paul Ryan, <sup>a</sup> Jan Balajka, <sup>a</sup> Margareta Wagner, <sup>a</sup> Matthias Meier, <sup>c</sup> Cesare Franchini, <sup>cd</sup> Gianfranco Pacchioni, <sup>e</sup> Ulrike Diebold, <sup>a</sup> Michael Schmid, <sup>a</sup> Florian Libisch, <sup>b</sup> Jiří Pavelec <sup>\*a</sup> and Gareth S. Parkinson

Gem-dicarbonyls of transition metals supported on metal (oxide) surfaces are common intermediates in heterogeneous catalysis. While infrared (IR) spectroscopy is a standard tool for detecting these species on powder catalysts, the ill-defined crystallographic environment renders data interpretation challenging. In this work, we apply a multi-technique surface science approach to investigate rhodium gem-dicarbonyls on a single-crystalline rutile  $\text{TiO}_2(110)$  surface. We combine spectroscopy, scanning probe microscopy, and density functional theory (DFT) to determine their location and coordination on the surface. IR spectroscopy shows the successful creation of gem-dicarbonyls on a titania single crystal by exposing deposited Rh atoms to CO gas, followed by annealing to 200–250 K. Low-temperature scanning tunneling microscopy (STM) and non-contact atomic force microscopy (nc-AFM) data reveal that these complexes are mostly aligned along the [001] crystallographic direction, corroborating theoretical predictions. Notably, X-ray photoelectron spectroscopy (XPS) data reveal multiple rhodium species on the surface, even when the IR spectra show only the signature of rhodium gem-dicarbonyls. As such, our results highlight the complex behavior of carbonyls on metal oxide surfaces, and demonstrate the necessity of multi-technique approaches for the adequate characterization of single-atom catalysts.

Received 2nd July 2025  
Accepted 7th October 2025

DOI: 10.1039/d5sc04889c  
[rsc.li/chemical-science](http://rsc.li/chemical-science)

## 1 Introduction

Transition metal carbonyl compounds, including those of Rh, Pd, and Pt, play a pivotal role in both homogeneous and heterogeneous catalysis.<sup>1</sup> Their utility arises from the strength of the metal–CO bond, which is strong enough to stabilize the compound yet weak enough to render CO an exchangeable ligand. As a result, transition metal carbonyls are established catalysts for a number of processes, such as acetic acid synthesis, hydroformylation, Reppe chemistry, and polymerization reactions.<sup>2</sup> Metal carbonyls are also integral to the field of single-atom catalysis (SAC). An isolated single atom is typically prone to sintering when it lacks sufficient coordination on the surface, but can be stabilized by coordinating to suitable ligands. Transition metal carbonyls are therefore a direct link between homogeneous and heterogeneous SAC, since the single

atom anchored to the surface resembles a metal complex with (exchangeable) ligands.<sup>3–6</sup> Hence, transition metal carbonyls are garnering significant attention as precursors or intermediates in SAC systems.<sup>7</sup> For noble metals like Pt, Ir, Pd, and Rh, single-atom dicarbonyls are frequently observed on supports such as zeolites, alumina, ceria, and titania.<sup>7–9</sup> These species, often referred to as geminal (gem)-dicarbonyls, have been extensively studied, particularly in the case of Rh due to its relevance in, *e.g.*, catalytic converters or the hydroformylation reaction.<sup>10–12</sup> IR spectroscopy has been the primary technique for detecting gem-dicarbonyls, which yield two characteristic peaks originating from the symmetric and asymmetric vibrational modes of the CO molecules. For Rh, these are typically located between 2120–2075  $\text{cm}^{-1}$  and 2053–1989  $\text{cm}^{-1}$ , respectively.<sup>9</sup> Recently, Rh carbonyl species have once more received considerable attention as surface species involved in catalytic reactions.<sup>13–19</sup> Christopher and co-workers have expanded the scope by experimental and computational studies of Rh gem-dicarbonyls on various metal oxide supports for applied catalysis.<sup>17,20,21</sup> Their works elucidate the creation and stability of Rh carbonyls under various conditions. This includes a study of different Rh carbonyls on rutile  $\text{TiO}_2$  that form after activation of the catalyst by heating in CO. Complementary DFT calculations by Sautet

<sup>a</sup>Institute of Applied Physics, TU Wien, Vienna, Austria. E-mail: [pavelec@iap.tuwien.ac.at](mailto:pavelec@iap.tuwien.ac.at); [eder@iap.tuwien.ac.at](mailto:eder@iap.tuwien.ac.at)

<sup>b</sup>Institute of Theoretical Physics, TU Wien, Vienna, Austria

<sup>c</sup>Faculty of Physics and Center for Computational Materials Science, University of Vienna, Vienna, Austria

<sup>d</sup>Dipartimento di Fisica e Astronomia, Università di Bologna, Bologna, Italy

<sup>e</sup>Department of Materials Science, University of Milano-Bicocca, Milano, Italy



and co-workers shed light on their relative stability as a function of the chemical potentials of  $O_2$  and CO.<sup>16</sup> This particular work demonstrated how Rh adatoms adapt to the conditions dictated by the environment, and that the gem-dicarbonyl is the dominant form under reducing conditions in the presence of CO. Despite these advancements in understanding transition metal carbonyls on oxidic supports, comprehensive atomic-level studies using diverse experimental techniques remain scarce. IR spectroscopy remains the main tool for their investigation on powders; however, the IR spectral bands for gem-dicarbonyls in the literature span a range of approximately  $50\text{ cm}^{-1}$ , and band intensities can be unreliable as quantitative measures.<sup>9</sup> The transition dipole moment of a molecule determines its signal intensity and can differ vastly depending on the adsorption site and the interplay of donation and back-donation of electron density. This effect is especially pronounced for CO, making the use of additional analytic techniques particularly important for characterizing carbonyl species.<sup>7,9,22</sup> Moreover, conventional DFT methods to determine the calculated frequencies of the IR absorption bands are often inaccurate.<sup>23,24</sup> To address these challenges, this study employs a multi-technique approach on an idealized model system. Using a rutile  $TiO_2(110)$  single crystal in ultra-high vacuum (UHV), we leverage a newly developed infrared reflection absorption spectroscopy (IRAS) setup,<sup>25</sup> linking our findings to those in the literature with IR spectroscopy as a bridging technique. Complementary low-temperature STM and nc-AFM provide direct visualization of Rh gem-dicarbonyls on the surface, pinpointing their location and coordination on  $TiO_2(110)$ . Additionally, XPS data provide information about the chemical state of Rh on the surface. DFT calculations rationalize the experimental findings from IRAS and XPS. This comprehensive approach establishes a benchmark for Rh gem-dicarbonyls and underscores the potential pitfalls of relying solely on a single technique for characterizing (single-atom) surface species.

## 2 Results

### 2.1 IRAS spectra of Rh gem-dicarbonyls

**2.1.1 Experimental IRAS frequencies.** Two methods for synthesizing Rh gem-dicarbonyls on  $TiO_2(110)$  in UHV are reported in the literature, either by decomposing Rh clusters under high pressures of CO gas,<sup>26</sup> or by decomposing  $Rh(CO)_2Cl_2$  complexes.<sup>27</sup> However, the first approach was not possible in a clean fashion with our experimental setups, and the latter yields significant amounts of Cl on the surface, which we sought to avoid due to its potential impact on the electronic and geometric structures of the system.<sup>28</sup> We have shown previously that single Rh atoms can be immobilized on  $TiO_2(110)$  by evaporating Rh onto the surface at 80 K,<sup>29</sup> and we used this method as a basis to synthesize the Rh gem-dicarbonyls as illustrated in the following. Fig. 1 shows IRAS spectra of 0.05 ML Rh on  $TiO_2(110)$  deposited at 80 K before and after CO adsorption. The spectra were recorded sequentially at 80 K. The accompanying annotations describe the specific sample treatments applied prior to each measurement.

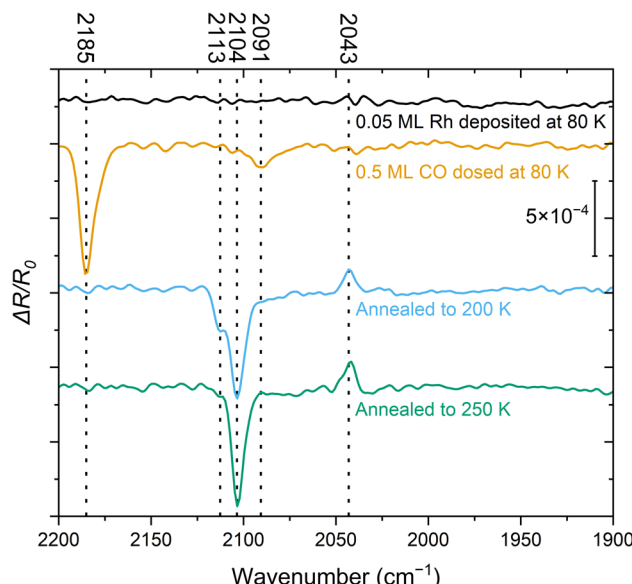


Fig. 1 IRAS spectra (baseline-corrected, obtained with p-polarized light, [001] direction in the incidence plane,  $4\text{ cm}^{-1}$  resolution, 60 kHz mirror velocity, 4000 scans recorded over  $\approx 10$  min at 80 K for each spectrum) of 0.05 ML Rh deposited at 80 K on  $TiO_2(110)$  (black trace), with additional 0.5 ML CO dosed at 80 K (orange trace), after heating to 200 K (blue trace), and after heating to 250 K (green trace). The peaks at  $2104\text{ cm}^{-1}$  and  $2043\text{ cm}^{-1}$  are assigned to the symmetric and asymmetric vibrational modes of the Rh gem-dicarbonyl, respectively. The reference spectrum was recorded before the series and used for all subsequent measurements.

The spectrum recorded immediately after Rh deposition at 80 K (Fig. 1, black) does not show any detectable features in the relevant wavenumber range of  $2200\text{--}1900\text{ cm}^{-1}$  where the CO-stretch vibration of transition metal carbonyls is commonly found. This indicates that CO adsorption from the residual gas in the UHV chamber is negligible. After adding 0.5 ML CO at 80 K (Fig. 1, orange), we identify two signals: an intense peak at  $2185\text{ cm}^{-1}$ , attributed to CO on  $TiO_2(110)$ ,<sup>25,30</sup> and a band around  $2091\text{ cm}^{-1}$ . The latter falls within a region where multiple species of Rh carbonyls have been postulated on metal oxides and zeolites.<sup>9,31,32</sup> The rather broad peak suggests a mixture of species. After flashing the sample to 200 K and cooling it back to 80 K (Fig. 1, blue), the CO/ $TiO_2(110)$  peak has disappeared, consistent with the desorption of CO from this surface at  $\approx 150$  K.<sup>30</sup> Furthermore, the feature at  $2091\text{ cm}^{-1}$  is no longer present. Instead, we observe three species at  $2113\text{ cm}^{-1}$ ,  $2104\text{ cm}^{-1}$ , and  $2043\text{ cm}^{-1}$ . The latter two are characteristic of the Rh gem-dicarbonyl<sup>27</sup> and align with the expected parallel and perpendicular contributions of p-polarized light over the measured angular range.<sup>25</sup> The azimuthal orientation of the gem-dicarbonyls on single-crystalline metal oxides can therefore be inferred from the IR data, since the surface selection rule that governs reflectivity on metallic surfaces does not apply to dielectric substrates.<sup>25,27,30,33,34</sup> In our setup, the principal ray of the IR beam projected onto the surface is parallel to [001], *i.e.*, parallel to the Ti and O rows. The azimuthal orientation of the gem-



dicarbonyls on single-crystalline metal oxides can be inferred from the appearance of the positive  $\Delta R/R_0$  peak; this peak would not appear in p-polarization for asymmetric stretch in the  $[1\bar{1}0]$  direction (an azimuthal orientation of the gem-dicarbonyl perpendicular to the Ti and O rows). When Rh dicarbonyls are measured on powders whose surfaces are randomly oriented, these two peaks are observed as two minima of the reflectance (maxima of absorbance) in IR spectra. However, our IR beam is reflected on a single crystal surface at a well-defined range of incidence angles, chosen such that the symmetric ( $2104\text{ cm}^{-1}$ ) and asymmetric stretch ( $2043\text{ cm}^{-1}$ ) result in a lower and higher reflectivity, respectively. This results from the orientation of the dipole moments and the Fresnel equations, as confirmed by simulations.<sup>25</sup> Following annealing to 250 K (Fig. 1, green trace) the  $2113\text{ cm}^{-1}$  feature disappears, while the other two signals associated with the gem-dicarbonyl remain. We cannot assign the peak at  $2113\text{ cm}^{-1}$  to one certain species at this point, but we attribute it to a metastable Rh-carbonyl species.<sup>9,31</sup> By annealing to room temperature and above (Fig. S1), the Rh dicarbonyls disappear and a band around  $2020\text{--}2040\text{ cm}^{-1}$  emerges, where CO on metallic Rh is typically located.<sup>35</sup> This is clear evidence that the previously observed Rh species have aggregated to form CO-covered Rh clusters. While we have observed these vibrational frequencies of the carbonyl species most frequently in our experiments, we have occasionally observed a slight shift of  $1\text{--}4\text{ cm}^{-1}$  towards higher wave-numbers. We ascribe this to differences in the preparation procedure, and to an enhanced number of adsorbates from the residual gas of the UHV chamber, interacting with the gem-dicarbonyls when the adsorbates are in close proximity to them.

An alternative synthetic route towards the Rh gem-dicarbonyls involves depositing Rh onto a CO-covered  $\text{TiO}_2(110)$  surface. This approach has been successfully employed for creating Fe complexes on ligand-covered  $\text{FeO}(111)$  single crystals.<sup>36,37</sup> Fig. S2 shows the corresponding IRAS spectra. This method results in the formation of multiple Rh carbonyl species, even after annealing. It hence appears less effective for the selective synthesis of a single type of Rh gem-dicarbonyl on  $\text{TiO}_2(110)$ .

**2.1.2 DFT calculations on Rh gem-dicarbonyls.** The optimized ground-state structure of the Rh gem-dicarbonyl was determined using DFT+*U* calculations. Fig. 2c illustrates its arrangement on the  $\text{TiO}_2(110)$  surface: the Rh atom (light grey) is positioned between two bridge-bonded O anions (red). The two CO molecules (with C in black) attached to the Rh atom are aligned parallel to the  $[001]$  direction. This is the lowest-energy Rh gem-dicarbonyl configuration found in our calculations and in an earlier work by Sautet and co-workers.<sup>16</sup> The adsorption energy per CO molecule in the square-planar geometry is energetically more favorable by nearly 0.65 eV compared to the tetrahedral alternative, in which the CO molecules are aligned perpendicular to the O and Ti rows (Fig. S3). The calculated Bader charge of the Rh in the gem-dicarbonyl of Fig. 2c is  $+0.68e$ , which is typical for a  $\text{Rh}^{1+}$  state. This means that one Ti atom in the subsurface layer is reduced from  $\text{Ti}^{4+}$  to  $\text{Ti}^{3+}$ .<sup>29,38</sup> These findings align with the well-known preference of Rh<sup>+</sup>

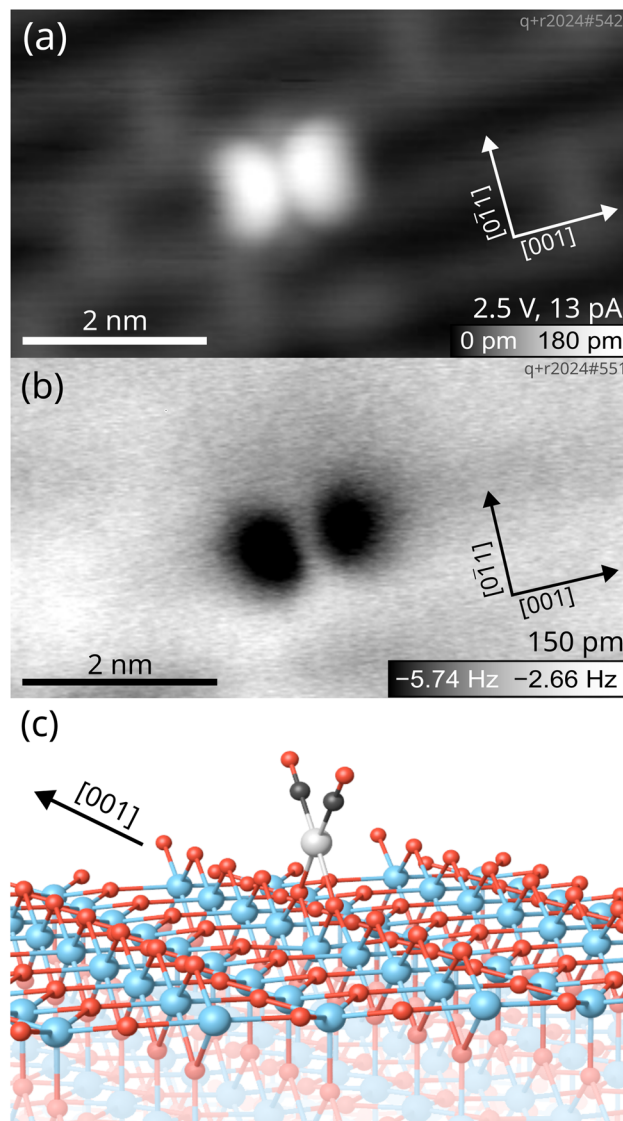


Fig. 2 Low-temperature scanning probe images of a Rh gem-dicarbonyl on  $\text{TiO}_2(110)$  taken at 14 K with a Cu-terminated tip. (a) Empty-states STM image showing the two CO molecules of the Rh gem-dicarbonyl appearing as bright lobes on the  $\text{TiO}_2(110)$  surface. (b) Constant-height nc-AFM image of the same gem-dicarbonyl with a metallic tip, imaging the two CO molecules as dark blobs due to the attractive interaction between the metal tip and the O atoms of the CO (amplitude = 150 pm,  $U = 0.0\text{ V}$ ). (c) The optimized structure of the Rh gem-dicarbonyl on the  $\text{TiO}_2(110)$  surface obtained by DFT+*U* calculations (Ti: blue; O: red; C: black; Rh: grey).

complexes for square-planar over tetrahedral geometries, as observed in various coordination compounds.<sup>39</sup>

Our calculated CO vibrational frequencies are  $2098.9\text{ cm}^{-1}$  and  $2042.6\text{ cm}^{-1}$  at the HSE06 level ( $2080\text{ cm}^{-1}$  and  $2021\text{ cm}^{-1}$  with the optPBE-vdW functional). These values agree with our experimental observations within the accuracy of DFT expected for such calculations, particularly regarding the difference between symmetric and asymmetric stretching modes ( $61\text{ cm}^{-1}$  in the experiment and 56 and  $59\text{ cm}^{-1}$  in the HSE06 and optPBE-vdW calculations, respectively). With optPBE-vdW, the



difference between the two modes exhibits a smaller error than their individual absolute frequency values due to error compensation from the shared approximation. We considered the possibility of Rh monocarbonyl species, but our calculated CO vibrational frequency with optPBE-vdW for a Rh monocarbonyl (Fig. S3) is  $2011\text{ cm}^{-1}$ , which is not observed in our experimental IR spectra. Therefore, we ascribe the IR peaks at  $2104\text{ cm}^{-1}$  and  $2043\text{ cm}^{-1}$  to the symmetric and asymmetric stretch of  $\text{Rh}^+(\text{CO})_2$ , respectively.

## 2.2 Rh gem-dicarbonyls in low-temperature scanning probe microscopy

To further confirm the conformation of Rh gem-dicarbonyls, we employed low-temperature STM and nc-AFM. Fig. 2 presents microscopy images taken at a sample temperature of 14 K. The sample was prepared by depositing 0.05 ML Rh onto the  $\text{TiO}_2(110)$  surface, followed by dosing 1 langmuir (L) of CO and annealing to  $\approx 270\text{ K}$ . An overview scan is presented in Fig. S4.

The overview scan in Fig. S4 shows the presence of clusters apart from the features we ascribe to the gem-dicarbonyls (green circles). We believe that the abundance of clusters is due to the fact that the annealing temperature in the STM experiment ( $\approx 270\text{ K}$ ) was higher than in the IR experiment ( $250\text{ K}$ ). However, it is plausible that clusters are present on the sample used in the IR experiment as well, but are not detected if they have no CO molecules adsorbed. In the empty-states STM image in Fig. 2a, we observe the characteristic features of the  $\text{TiO}_2(110)$  surface.<sup>40</sup> The grey and black rows along the [001] direction correspond to the Ti cations and bridge-bonded O anions, respectively. Grey bridges across the black rows are O vacancies,<sup>41</sup> evidence for a reduced, non-stoichiometric surface. We find a distinct feature in the form of a bright double-lobe oriented along the [001] direction, located on top of a bridge-bonded O row. The center of the lobes is exactly located between two bridging oxygen anions, as illustrated by the unit cell grid centered on the oxygen vacancies (see Fig. S5). The bright double lobe stems from the two CO molecules aligned in a plane parallel to the Ti and O rows, in excellent agreement with our spectroscopic and computational results, and calculations by Sautet and co-workers.<sup>16</sup> A nc-AFM image of the same spot on the surface in Fig. 2b corroborates this interpretation. We find again two lobes aligned in the [001] direction, which appear dark in this case due to the attractive interaction between the metallic Cu-terminated tip and the O of the CO molecules.

As mentioned above, the STM images show a substantial number of species attributed to  $\text{Rh}_n$  clusters at a Rh coverage of 0.05 ML and successive CO adsorption and annealing to  $\approx 270\text{ K}$ . By using the same preparation of Rh gem-dicarbonyls on the  $\text{TiO}_2(110)$  surface but aiming at a lower Rh coverage (0.005 ML, *i.e.*, one tenth of the previous coverage), the number of large clusters is reduced, but Rh clusters cannot be fully avoided. Fig. 3 shows SPM images of the surface after this preparation.

An overview scan covering a larger surface area (Fig. 3a) revealed Rh clusters as well as double-lobed, inequivalent

features apart from the typical surface species like hydroxyls and O vacancies. A constant-height image of a region of Fig. 3a shows an asymmetry of two gem-dicarbonyls, depicted in the frequency shift in Fig. 3b and the simultaneously recorded tunneling current in Fig. 3c. Under all imaging conditions, this asymmetry of the individual double-lobed features stays consistent. The opposite orientations of these inequivalent CO molecules suggest that the effect is not an artifact from a slightly asymmetric tip. Instead, the inequivalence could arise from distinct interactions between the two CO molecules of the dicarbonyl and the  $\text{TiO}_2(110)$  surface, causing a tilt of the structure in the [001] or [001] direction. One plausible explanation involves interaction with nearby OH groups, which are ubiquitous on  $\text{TiO}_2(110)$  surfaces. Our DFT calculations show that the interaction between one Rh-bound CO and a hydroxyl group on the O rows would indeed lead to an asymmetric position of the CO molecules with respect to the Rh atom (Fig. S6). Recent calculations for anatase  $\text{TiO}_2(001)$  by Christopher and Pacchioni lend support to this hypothesis, demonstrating that OH groups can interact with CO molecules, influencing their geometry and alignment.<sup>17</sup> We therefore assign the different size of the lobes in nc-AFM to a neighboring OH group next to one CO molecule of the Rh gem-dicarbonyl complex.

## 2.3 XPS spectra of Rh and C

To understand the chemical nature of the Rh species, we recorded XPS spectra during the same experiment as for the IRAS measurements depicted in Fig. 1. Fig. 4 presents XPS spectra of the Rh 3d and C 1s region of the  $\text{TiO}_2(110)$  surface at 80 K after various treatments, as indicated in the corresponding annotations.

The Rh 3d spectrum in Fig. 4a shows the expected doublet after depositing 0.05 ML Rh at 80 K (black trace). The Rh 3d<sub>5/2</sub> peak is centered around 308 eV, consistent with a prior study of this system.<sup>29</sup> The width of the peak suggests the coexistence of different species, presumably the single atoms and very small clusters as observed by STM/nc-AFM in Fig. S7. Due to the broadness of the peak, the presence of metallic Rh, centered around 307.7 eV (Fig. S8) seems likely. Adding 0.5 ML CO at 80 K (Fig. 4a, orange trace), splits the Rh 3d<sub>5/2</sub> peak into two maxima of comparable intensity at 310.1 eV and 308.9 eV. Again, the broadness of both peaks, in particular the tail below 308.9 eV, suggests contributions from different chemical surroundings. Upon heating to 100 K, 150 K, and 200 K (yellow, dark blue, and light blue traces, respectively), we still observe the two species at the same position, although their relative intensities change. At these temperatures, the higher-binding-energy component dominates. At 250 K (green trace), the intensity shifts slightly in favor of the lower-binding-energy component, and a shoulder emerges at 308.2 eV, indicative of a larger, agglomerated species. The observation of the component around 308.2 eV is consistent with the observation of clusters in STM in Fig. S4. After annealing to 300 K (pink trace in Fig. 4a), the species at 308.2 eV dominates, with diminished intensities for the two components at higher binding energy. The substantial



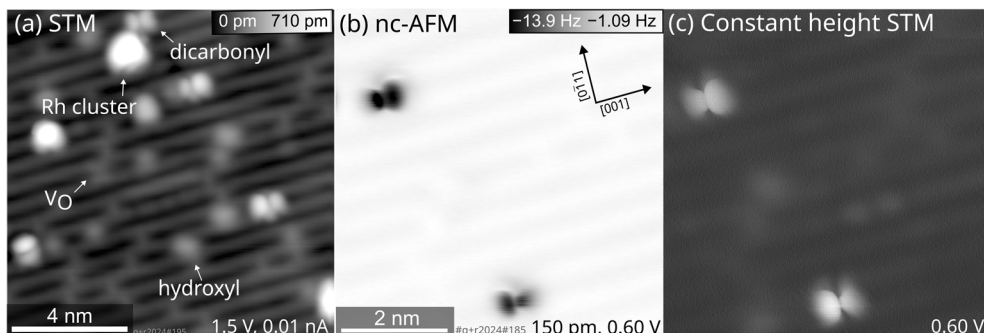


Fig. 3 Low-temperature SPM images of Rh gem-dicarbonyls on  $\text{TiO}_2(110)$  acquired at 14 K with a Cu-terminated tip. 0.005 ML Rh were deposited at 100 K, exposed to 1 langmuir (L) (corresponding to  $\approx 0.88$  ML) CO at 100 K, and heated to 270 K. (a) Empty-states STM image of a  $15 \text{ nm} \times 15 \text{ nm}$  area. (b) Constant-height nc-AFM image of a region of (a) containing two gem-dicarbonyls with a metallic tip, imaging the two CO molecules as black spots due to their attractive interaction to the tip (amplitude = 150 pm). (c) Constant-height STM image of the same area acquired at the same time as the nc-AFM scan.

reduction in the intensity of the peak at 310.1 eV coincides with the loss of the bands from the gem-dicarbonyl in IRAS. Thus, we assign the peak at 310.1 eV to the Rh gem-dicarbonyl, and the species around 308.9 eV to clustered Rh-carbonyl species. This observation aligns well with a study by Hayden *et al.*,<sup>42</sup> who observed the agglomeration of Rh gem-dicarbonyls on  $\text{TiO}_2(110)$  at room temperature; this was attributed to the impact of hydrogen (*i.e.*, hydroxyl groups) on the surface. Our result also aligns with observations by Frederick *et al.*, who found a similar Rh 3d binding energy (310.2 eV) for Rh gem-dicarbonyls on alumina.<sup>43</sup> The lower binding energy component at 308.9 eV likely originates from the carbonylation of small Rh clusters that formed upon deposition, as depicted in Fig. S7. The variety of Rh species in Fig. 4a is much larger after annealing to 300 K compared to depositing Rh directly at 300 K (see Fig. S8). XPS of the latter yields only one significant Rh 3d<sub>5/2</sub> peak at a neutral Rh position of 307.7 eV, originating from clusters as detected in STM.<sup>29</sup> After heating to 400 K (red in

Fig. 4a), we find one pronounced species around 308 eV, close to the initial position after Rh deposition in the absence of CO. This peak is assigned to Rh clusters with a more metallic character. DFT core-level calculations using the initial-state approximation reveal that the binding energies of Rh 3d for a Rh monocarbonyl and a Rh gem-dicarbonyl are shifted to higher values by 0.79 and 1.46 eV, respectively, relative to the Rh single-atomic ground-state configuration on  $\text{TiO}_2(110)$ . The Rh 3d<sub>5/2</sub> peak position around 310 eV attributed to the gem-dicarbonyl could be taken as representative of a  $\text{Rh}^{3+}$  charge state. However, the Bader charge analysis and the number of reduced Ti atoms indicate that this Rh species is in the  $\text{Rh}^+$  state. Hence, the shift of the Rh peaks towards higher binding energies upon CO exposure is due to intramolecular redistribution of electron density, but not due to a change in formal charge state. This is in line with other single-atomic carbonyls on  $\text{Fe}_3\text{O}_4(001)$ .<sup>44</sup> Our DFT results (Fig. S9) show that increasing the Rh coordination by binding to the CO molecules in the

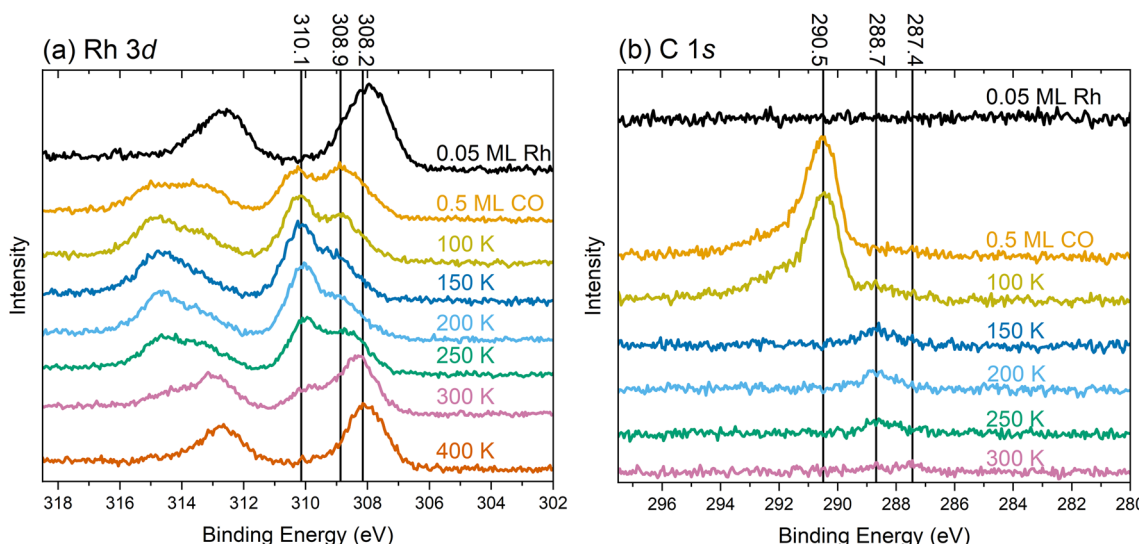


Fig. 4 XPS spectra of (a) the Rh 3d and (b) C 1s regions taken at 80 K using monochromatized  $\text{Al K}_\alpha$  radiation at  $70^\circ$  grazing emission for enhanced surface sensitivity. The colored text corresponding to each spectrum indicates the treatment before the measurement.



square-planar configuration shifts the energies of d-band states to lower values compared to adsorbed, bare Rh. This also suggests that the available mobile charge around the Fermi edge to screen out the core hole is substantially reduced at the Rh site. In addition to initial-state effects such as an overall downshift of the Rh states, this could also lead to final state effects. The C 1s spectra in Fig. 4b exhibit no detectable signal for the Rh-decorated surface (black trace). Following CO dosing (orange trace), a peak emerges at 290.5 eV, which we ascribe to CO adsorbed on  $\text{TiO}_2$ . Heating to 100 K (yellow trace) induces a shoulder at 288.7 eV, which we ascribe to CO on Rh. This corroborates evidence from IRAS (Fig. 1, orange trace) which suggests that CO is immobile after landing on the surface at 80 K. Hence, it requires thermal energy to facilitate CO diffusion, and to lift a Rh atom onto the bridging O rows (see Fig. S9a to S9b) to form Rh gem-dicarbonyls (Fig. S9c). After annealing to 150 K (Fig. 4b dark blue trace), the peak of CO on  $\text{TiO}_2$  (290.5 eV) has vanished due to CO desorption from the substrate. This agrees again with the corresponding result in the IR spectra in Fig. 1 (blue trace) and the literature.<sup>30</sup> When increasing the temperature to 200 K and 250 K (light blue and green trace in Fig. 4b, respectively), the CO/Rh peak at 288.7 eV remains stable in position and intensity. At 300 K, we find its intensity diminished, due to the desorption of the CO from the Rh gem-dicarbonyls. This coincides with the emergence of a weak peak around 287.4 eV. This new signal is attributed to CO adsorbed on Rh clusters, reflecting the aggregation of Rh species as observed in the Rh 3d spectra.

### 3 Discussion

The infrared spectra (Fig. 1) demonstrate the facile synthesis of Rh gem-dicarbonyls on  $\text{TiO}_2(110)$  in UHV, a model system for metal carbonyls anchored to metal oxides.<sup>9,45</sup> Our synthetic approach avoids high pressures and Cl contaminations on the surface (in contrast to previous works),<sup>27,46</sup> and is presumably transferable to other transition metals like Ir, Ni, Pt, or Pd, known for forming carbonyl complexes on metal oxide surfaces.<sup>8,9,45</sup> Our study provides the first low-temperature scanning probe images of Rh gem-dicarbonyls on  $\text{TiO}_2(110)$  (Fig. 2). The double-lobed features, aligned along the [001] direction, strongly support a square-planar geometry. This finding contrasts with earlier studies by Hayden *et al.*, which provide evidence for a perpendicular alignment of the Rh gem-dicarbonyls to the Ti and O rows on  $\text{TiO}_2(110)$  after dosing  $[\text{Rh}(\text{CO})_2(\text{Cl})_2]$ .<sup>33</sup> However, our spectroscopic results in Fig. 1 are consistent with our computational results and recent work by Tang *et al.*, which predict the alignment along the bridging O rows on  $\text{TiO}_2(110)$ ,<sup>16</sup> as well as our SPM images. The square-planar geometry arises from the coordination of Rh with two CO ligands parallel to the Ti and O rows, reflecting the intrinsic preference of  $\text{Rh}^+$  complexes for square-planar over tetrahedral conformations.<sup>39</sup> We have observed distortions of the dicarbonyls (Fig. 3), possibly due to the interaction of CO ligands with surface OH groups, as suggested by DFT calculations (Fig. S6). These distortions could influence the catalytic activity and selectivity of gem-dicarbonyl species.<sup>47</sup> Our XPS data (Fig. 4)

provide critical insights into the electronic states of Rh species. Note that the Rh 3d peaks after deposition are located at higher binding energies ( $\approx 308$  eV for Rh 3d<sub>5/2</sub>) compared to neutral, bulk-like Rh ( $\approx 307$  eV),<sup>48</sup> likely due to final-state effects of the single adatoms and small clusters.<sup>29</sup> The broadness of the signal is in excellent agreement with the fact that we find single atoms as well as small clusters in STM after deposition. Exposing the Rh surface species to CO and heating this system creates Rh carbonyls from single atoms and possibly the partial break-up of clusters.<sup>49</sup> These processes are reflected in changes in the Rh 3d and C 1s spectra already at 80 K (CO exposure) and upon annealing to 100 K. The Rh 3d signal splits into components with lower and higher binding energy (Fig. 4a). The feature with higher binding energy at 310.1 eV is identified as originating from the gem-dicarbonyl, in agreement with the literature.<sup>43</sup> The 310.1 eV signal increases upon annealing up to 200–250 K. This reflects both enhanced CO diffusion to Rh sites and CO-induced restructuring of Rh species, including jumping onto the rows of 2-fold oxygen (Fig. S9a to S9b) and breaking up of small clusters.<sup>26,49</sup> This indicates that the Rh gem-dicarbonyls are thermodynamically favorable, but their formation is kinetically hampered at low temperatures. The authors of the work on Rh gem-dicarbonyls on alumina<sup>43</sup> ascribed the peak at  $\approx 310$  eV to a  $\text{Rh}^{3+}$  species, but our DFT results suggest that the Rh in the gem-dicarbonyl on  $\text{TiO}_2(110)$  is in the oxidation state 1+, and we consider a  $\text{Rh}^{3+}$  state unlikely on the hardly reducible alumina substrate. We also rule out the oxidation state 2+ for the Rh species due to the absence of multiplet splitting in the Rh 3d spectra.<sup>50</sup> The different Rh 3d binding energies with and without CO are rather due to electronic effects attributed to the different coordination, as confirmed by DFT (Fig. S9). The calculated vibration frequencies confirm that the two main peaks observed in the same temperature range as the dicarbonyl signal in XPS (Fig. 1,  $2104\text{ cm}^{-1}$  and  $2043\text{ cm}^{-1}$ ) are due to the dicarbonyl. The IRAS shows an additional signal at  $2113\text{ cm}^{-1}$  after annealing to 200 K, which disappears upon annealing to 250 K. We note that the disappearance coincides with a slight intensity increase of the gem-dicarbonyl peak at  $2104\text{ cm}^{-1}$ , but also with an increase of the Rh 3d XPS signal at  $\approx 308$  eV (Fig. 4a), which is related to small Rh clusters. Thus, it is unclear whether the species responsible for the  $2113\text{ cm}^{-1}$  peak transforms into the “normal” gem-dicarbonyl or creates Rh clusters upon its disappearance.

XPS suggests the presence of small Rh carbonyl clusters with a Rh 3d<sub>5/2</sub> binding energy around 308.9 eV. It seems surprising that the IRAS spectra do not show any evidence for their presence. However, this is likely due to the heterogeneity of these carbonyl clusters. For clusters with different sizes (different amounts of Rh and CO), the directions of the CO dipole moments and their vibrational frequencies vary substantially.<sup>51</sup> The resulting signals do not add coherently, and thus no distinct IR feature emerges. It is also possible that some of these Rh carbonyl clusters are overshadowed by the peak of the Rh gem-dicarbonyl asymmetric stretch at  $2043\text{ cm}^{-1}$ . In any event, upon annealing to temperatures above 250 K, the dicarbonyls vanish and the Rh forms small clusters. These observations are in line with studies proposing the reductive desorption of CO



from Rh carbonyls on zeolites,<sup>52</sup> and the presence of clusters in the STM images in Fig. 3 and S4. The peak intensities of the symmetric and asymmetric stretch in the IRAS spectrum in Fig. 1 are consistent with the calculated IRAS sensitivities for out-of-plane and in-plane vibrations with p-polarized light. According to previous calculations, IRAS is substantially more sensitive to out-of-plane vibrations at incidence angles above 30°.<sup>25</sup>

These results show that relying solely on IR spectroscopy for identifying surface species, for example in single-atom catalysis, can be deceiving. More Rh species can be found in the XPS than one would expect from the IR data showing only a single dicarbonyl species following the 250 K anneal. This is likely due to these IR-invisible species binding to very few or no CO molecules, or the dipole moment of those CO species being too low,<sup>22</sup> as well as the inhomogeneity not leading to sharp IRAS peaks. Integration of the C 1s peaks in Fig. 4b shows that after CO desorption from the oxide (150 K and higher), the area under the remaining CO signal amounts to about 10% of the initial signal after dosing 0.5 ML CO. However, if all Rh atoms (0.05 ML) were covered by 2 CO molecules, it should amount to 20%. This provides additional evidence that not all Rh species are gem-dicarbonyls, and that some Rh atoms have to be in clusters, as suggested above, based on the lower binding energy component of the Rh 3d signal. The fact that the IR spectroscopy does not detect these significant quantities of clustered species has profound implications for catalysis, especially in single-atom systems, where the catalytic role of single atoms *versus* minor concentrations of clusters is often debated. A multi-technique approach, as demonstrated here, is essential to resolve ambiguities and provide a comprehensive understanding of the active surface species.<sup>53</sup>

## 4 Conclusions

Our results build upon and expand previous findings on gem-dicarbonyls on metal oxide supports. While earlier studies have primarily relied on IR spectroscopy, our multi-technique approach provides a more nuanced characterization of these species. The direct visualization of gem-dicarbonyls *via* STM and nc-AFM bridges the gap between theoretical predictions and experimental evidence. Their stability under realistic operating conditions is limited, with decomposition of the dicarbonyls and formation of Rh clusters occurring at temperatures above 250 K. However, the transition metal gem-dicarbonyls on metal oxides with distinct spectroscopic fingerprints are important intermediates in catalytic processes in general, potentially influencing reaction pathways. Additionally, the suggested interaction with surface OH groups may provide a route for tuning their electronic and geometric properties, opening avenues for site-specific catalysis. The scanning probe images show mainly gem-dicarbonyls oriented along the [001] direction along the Ti and O rows, in agreement with the IRAS data and DFT calculations predicting a fourfold-planar coordination of Rh<sup>+</sup>. The XPS data show that there is more than one Rh species on the surface, attributed to small Rh clusters, invisible in the IR spectra despite being present in

considerable amounts and likely covered by CO at these temperatures. This demonstrates the necessity of multi-technique approaches in the investigation of single atoms and carbonyls, and therefore has important implications for single-atom catalysis.

## Author contributions

Moritz Eder: conceptualization, methodology, investigation, original draft, review & editing, project administration. Faith Lewis: investigation, data curation, discussion. Johanna Hüttner: investigation, discussion. Jan Balajka: supervision, discussion. David Rath: investigation & discussion. Panukorn Sombut, Maosheng Hao: investigation, formal analysis, discussion. Matthias Meier, Florian Libisch, Cesare Franchini: supervision, discussion. Gianfranco Pacchioni: methodology, discussion. Jiri Pavleč: conceptualization, writing – review & editing, supervision, project administration. Paul Ryan, Margareta Wagner: discussion, validation. Michael Schmid, Ulrike Diebold, Gareth S. Parkinson: validation, resources, writing – review & editing, funding acquisition, discussion.

## Conflicts of interest

There are no conflicts to declare.

## Data availability

The data that support the findings of this study are available from the corresponding author upon reasonable request.

Supplementary information is available. See DOI: <https://doi.org/10.1039/d5sc04889c>.

## Acknowledgements

Funding from the European Research Council (ERC) under the European Union's Horizon 2020 research and innovation program (grant agreement no. 864628, Consolidator Research Grant "E-SAC") is acknowledged. This work was supported by the European Research Council under the European Union's Horizon 2020 research and innovation program (grant agreement no. 883395, Advanced Research Grant "WatFun"). This research was funded in part by the Austrian Science Fund (FWF) 10.55776/F81 and the Cluster of Excellence MECS (10.55776/COE5). For open access purposes, the authors have applied a CC BY public copyright license to any author accepted manuscript version arising from this submission. Moritz Eder acknowledges funding by the Marie Skłodowska-Curie Actions (Project 101103731, SCI-PHI). Matthias Meier gratefully acknowledges financial support from the Austrian Science Fund (FWF) (through project number 10.55776/PAT2176923). The computational results have been achieved using the Vienna Scientific Cluster (VSC). The authors acknowledge TU Wien Bibliothek for the financial support through its Open Access Funding Programme.



## References

- 1 P. J. Dyson and J. S. McIndoe, *Transition Metal Carbonyl Cluster Chemistry*, CRC Press, 2018.
- 2 C. Masters, *Homogeneous Transition-metal Catalysis*, Springer Netherlands, Dordrecht, 1980.
- 3 F. Chen, X. Jiang, L. Zhang, R. Lang and B. Qiao, Single-atom catalysis: Bridging the homo- and heterogeneous catalysis, *Chin. J. Catal.*, 2018, **39**(5), 893–898.
- 4 F. Kraushofer, L. Haager, M. Eder, A. Rafsanjani-Abbas, Z. Jakub, G. Franceschi, M. Riva, M. Meier, M. Schmid, U. Diebold and G. S. Parkinson, Single Rh Adatoms Stabilized on  $\alpha$ -Fe<sub>2</sub>O<sub>3</sub>(1102) by Coadsorbed Water, *ACS Energy Lett.*, 2022, **7**(1), 375–380.
- 5 F. Kraushofer and G. S. Parkinson, Single-Atom Catalysis: Insights from Model Systems, *Chem. Rev.*, 2022, **122**(18), 14911–14939.
- 6 G. S. Parkinson, “Single-atom” catalysis: An opportunity for surface science, *Surf. Sci.*, 2025, **754**, 122687.
- 7 S. K. Kaiser, Z. Chen, D. Faust Akl, S. Mitchell and J. Pérez-Ramírez, Single-Atom Catalysts across the Periodic Table, *Chem. Rev.*, 2020, **120**(21), 11703–11809.
- 8 M. Frank, M. Bäumer, R. Kühnemuth and H. J. Freund, Metal Atoms and Particles on Oxide Supports: Probing Structure and Charge by Infrared Spectroscopy, *J. Phys. Chem. B*, 2001, **105**(36), 8569–8576.
- 9 K. I. Hadjiivanov and G. N. Vayssilov, Characterization of oxide surfaces and zeolites by carbon monoxide as an IR probe molecule, *Adv. Catal.*, 2002, 307–511.
- 10 C. G. C. W. Yang, Infrared studies of carbon monoxide chemisorbed on rhodium, *J. Phys. Chem.*, 1957, **61**(11), 1504.
- 11 J. A. Anderson, Infrared Study of CO Oxidation over Pt-Rh/Al<sub>2</sub>O<sub>3</sub> Catalysts, *J. Catal.*, 1993, **142**(1), 153–165.
- 12 S. S. C. Chuang, G. Srinivas and A. Mukherjee, Infrared Studies of the Interactions of C<sub>2</sub>H<sub>4</sub> and H<sub>2</sub> with Rh<sup>+</sup>(CO)<sub>2</sub> and CO Adsorbed on RhCl<sub>3</sub>/SiO<sub>2</sub> and Rh(NO<sub>3</sub>)<sub>3</sub>/SiO<sub>2</sub>, *J. Catal.*, 1993, **139**(2), 490–503.
- 13 Y. Kwon, T. Y. Kim, G. Kwon, J. Yi and H. Lee, Selective Activation of Methane on Single-Atom Catalyst of Rhodium Dispersed on Zirconia for Direct Conversion, *J. Am. Chem. Soc.*, 2017, **139**(48), 17694–17699.
- 14 C. Y. Fang, S. Zhang, Y. Hu, M. Vasiliu, J. E. Perez-Aguilar, E. T. Conley, D. A. Dixon, C.-Y. Chen and B. C. Gates, Reversible Metal Aggregation and Redispersion Driven by the Catalytic Water Gas Shift Half-Reactions: Interconversion of Single-Site Rhodium Complexes and Tetrarhodium Clusters in Zeolite HY, *ACS Catal.*, 2019, **9**(4), 3311–3321.
- 15 M. J. Hülsey, B. Zhang, Z. Ma, H. Asakura, D. A. Do, W. Chen, T. Tanaka, P. Zhang, Z. Wu and N. Yan, In situ spectroscopy-guided engineering of rhodium single-atom catalysts for CO oxidation, *Nat. Commun.*, 2019, **10**(1), 1330.
- 16 Y. Tang, C. Asokan, M. Xu, G. W. Graham, X. Pan, P. Christopher, J. Li and P. Sautet, Rh single atoms on TiO<sub>2</sub> dynamically respond to reaction conditions by adapting their site, *Nat. Commun.*, 2019, **10**(1), 4488.
- 17 C. Asokan, H. V. Thang, G. Pacchioni and P. Christopher, Reductant composition influences the coordination of atomically dispersed Rh on anatase TiO<sub>2</sub>, *Catal. Sci. Technol.*, 2020, **10**(6), 1597–1601.
- 18 F. Gu, X. Qin, M. Li, Y. Xu, S. Hong, M. Ouyang, G. Giannakakis, S. Cao, M. Peng, J. Xie, M. Wang, D. Han, D. Xiao and X. Wang, Selective Catalytic Oxidation of Methane to Methanol in Aqueous Medium over Copper Cations Promoted by Atomically Dispersed Rhodium on TiO<sub>2</sub>, *Angew. Chem., Int. Ed.*, 2022, **61**(18), e202201540.
- 19 S. Marino, L. Wei, M. Cortes-Reyes, Y. Cheng, P. Laing, G. Cavataio, C. Paolucci and W. Epling, Rhodium Catalyst Structural Changes during, and Their Impacts on the Kinetics of CO Oxidation, *JACS Au*, 2023, **3**(2), 459–467.
- 20 E. K. Schroeder, J. Finzel and P. Christopher, Photolysis of Atomically Dispersed Rh/Al<sub>2</sub>O<sub>3</sub> Catalysts: Controlling CO Coverage *in Situ* and Promoting Reaction Rates, *J. Phys. Chem. C*, 2022, **126**(43), 18292–18305.
- 21 J. Zhang, C. Asokan, G. Zakem, P. Christopher and J. W. Medlin, Enhancing sintering resistance of atomically dispersed catalysts in reducing environments with organic monolayers, *Green Energy Environ. Technol.*, 2022, **7**(6), 1263–1269.
- 22 T. L. Brown and D. J. Darensbourg, Intensities of CO stretching modes in the infrared spectra of adsorbed CO and metal carbonyls, *Inorg. Chem.*, 1967, **6**(5), 971.
- 23 P. G. Lustemberg, P. N. Plessow, Y. Wang, C. Yang, A. Nefedov, F. Studt, C. Wöll and M. V. Ganduglia-Pirovano, Vibrational Frequencies of Cerium-Oxide-Bound CO: A Challenge for Conventional DFT Methods, *Phys. Rev. Lett.*, 2020, **125**(25), 256101.
- 24 M. V. Ganduglia-Pirovano, A. Martínez-Arias, S. Chen, Y. Wang and P. G. Lustemberg, Comment on “Surface characterization of cerium oxide catalysts using deep learning with infrared spectroscopy of CO.”, *Mater. Today Sustain.*, 2024, **26**, 100783.
- 25 D. Rath, V. Mikerásek, C. Wang, M. Eder, M. Schmid, U. Diebold, G. S. Parkinson and J. Pavělec, Infrared reflection absorption spectroscopy setup with incidence angle selection for surfaces of non-metals, *Rev. Sci. Instrum.*, 2024, **95**(6), 065106.
- 26 A. Berkó and F. Solymosi, Adsorption-Induced Structural Changes of Rh Supported by TiO<sub>2</sub>(110)-(1×2): An STM Study, *J. Catal.*, 1999, **183**(1), 91–101.
- 27 J. Evans, B. Hayden, F. Mosselmans and A. Murray, Rhodium geminal dicarbonyl on TiO<sub>2</sub> (110), *J. Am. Chem. Soc.*, 1992, **114**(17), 6912.
- 28 D. I. Kondarides, Z. Zhang and X. E. Verykios, Chlorine-Induced Alterations in Oxidation State and CO Chemisorptive Properties of CeO<sub>2</sub>-Supported Rh Catalysts, *J. Catal.*, 1998, **176**(2), 536–544.
- 29 P. Sombut, L. Puntscher, M. Atzmueller, Z. Jakub, M. Reticcioli, M. Meier, G. S. Parkinson and C. Franchini, Role of Polarons in Single-Atom Catalysts: Case Study of Me<sub>1</sub> [Au<sub>1</sub>, Pt<sub>1</sub>, and Rh<sub>1</sub>] on TiO<sub>2</sub>(110), *Top. Catal.*, 2022, **65**(17–18), 1620–1630.



30 N. G. Petrik and G. A. Kimmel, Adsorption Geometry of CO versus Coverage on  $\text{TiO}_2(110)$  from s- and p-Polarized Infrared Spectroscopy, *J. Phys. Chem. Lett.*, 2012, **3**(23), 3425–3430.

31 C. A. Rice, S. D. Worley, C. W. Curtis, J. A. Guin and A. R. Tarrer, The oxidation state of dispersed Rh on  $\text{Al}_2\text{O}_3$ , *J. Phys. Chem.*, 1981, **74**(11), 6487–6497.

32 G. N. Vayssilov and N. Rösch, A New Interpretation of the IR Bands of Supported Rh(I) Monocarbonyl Complexes, *J. Am. Chem. Soc.*, 2002, **124**(14), 3783–3786.

33 B. E. Hayden, A. King and M. A. Newton, The alignment of a surface species determined by FT-RAIRS: rhodium gem-dicarbonyl on  $\text{TiO}_2(110)$ , *Chem. Phys. Lett.*, 1997, **269**(5), 485–488.

34 Y. Wang and C. Wöll, IR spectroscopic investigations of chemical and photochemical reactions on metal oxides: bridging the materials gap, *Chem. Soc. Rev.*, 2017, **46**(7), 1875–1932.

35 G. Krenn, I. Bako and R. Schennach, CO adsorption and CO and O coadsorption on Rh(111) studied by reflection absorption infrared spectroscopy and density functional theory, *J. Chem. Phys.*, 2006, **124**(14), 144703.

36 G. S. Parkinson, Z. Dohnálek, R. S. Smith and B. D. Kay, Reactivity of  $\text{C}_2\text{Cl}_6$  and  $\text{C}_2\text{Cl}_4$  Multilayers with  $\text{Fe}^0$  Atoms over  $\text{FeO}(111)$ , *J. Phys. Chem. C*, 2009, **113**(23), 10233–10241.

37 G. S. Parkinson, Z. Dohnálek, R. S. Smith and B. D. Kay, Reactivity of  $\text{Fe}^0$  Atoms with Mixed  $\text{CCl}_4$  and  $\text{D}_2\text{O}$  Films over  $\text{FeO}(111)$ , *J. Phys. Chem. C*, 2010, **114**(40), 17136–17141.

38 M. Reticcioli, M. Setvin, M. Schmid, U. Diebold and C. Franchini, Formation and dynamics of small polarons on the rutile  $\text{TiO}_2(110)$  surface, *Phys. Rev. B*, 2018, **98**(4), 045306.

39 G. K. Anderson and R. J. Cross, Isomerisation mechanisms of square-planar complexes, *Chem. Soc. Rev.*, 1980, **9**(2), 185–215.

40 U. Diebold, The surface science of titanium dioxide, *Surf. Sci. Rep.*, 2003, **48**(5–8), 53–229.

41 U. Diebold, J. F. Anderson, K. O. Ng and D. Vanderbilt, Evidence for the Tunneling Site on Transition-Metal Oxides:  $\text{TiO}_2(110)$ , *Phys. Rev. Lett.*, 1996, **77**(7), 1322–1325.

42 B. E. Hayden, A. King and M. A. Newton, The reaction of hydrogen with  $\text{TiO}_2(110)$  supported rhodium gem-dicarbonyl, *Surf. Sci.*, 1998, **397**(1–3), 306–313.

43 B. G. Frederick, G. Apai and T. N. Rhodin, An x-ray photoelectron spectroscopy study of rhodium carbonyls adsorbed on planar aluminas: formation of geminal dicarbonyl species, *J. Am. Chem. Soc.*, 1987, **109**(16), 4797–4803.

44 J. Hulva, M. Meier, R. Bliem, Z. Jakub, F. Kraushofer, M. Schmid, U. Diebold, C. Franchini and G. S. Parkinson, Unraveling CO adsorption on model single-atom catalysts, *Science*, 2021, **371**(6527), 375–379.

45 M. Babucci, A. Guntida and B. C. Gates, Atomically Dispersed Metals on Well-Defined Supports including Zeolites and Metal–Organic Frameworks: Structure, Bonding, Reactivity, and Catalysis, *Chem. Rev.*, 2020, **120**(21), 11956–11985.

46 J. Evans, B. E. Hayden, J. F. W. Mosselmans and A. J. Murray, Model Catalyst Studies of Titania Supported Rhodium, in *Elementary Reaction Steps in Heterogeneous Catalysis*, Springer Netherlands, Dordrecht, 1993, pp. 179–195.

47 H. H. Lamb, B. C. Gates and H. Knözinger, Molecular Organometallic Chemistry on Surfaces: Reactivity of Metal Carbonyls on Metal Oxides, *Angew. Chem., Int. Ed.*, 1988, **27**(9), 1127–1144.

48 L. A. DeLouise, E. J. White and N. Winograd, Characterization of CO binding sites on Rh{111} and Rh{331} surfaces by XPS and LEED: Comparison to EELS results, *Surf. Sci.*, 1984, **147**(1), 252–262.

49 R. R. Cavanagh and J. T. Yates, Site distribution studies of Rh supported on  $\text{Al}_2\text{O}_3$ —An infrared study of chemisorbed CO, *J. Chem. Phys.*, 1981, **74**(7), 4150–4155.

50 M. A. Isaacs, A. Graf and D. J. Morgan, XPS Insight Note: Multiplet Splitting in X-Ray Photoelectron Spectra, *Surf. Interface Anal.*, 2025, **57**(4), 285–290.

51 A. D. Brathwaite, H. L. Abbott-Lyon and M. A. Duncan, Distinctive Coordination of CO vs  $\text{N}_2$  to Rhodium Cations: An Infrared and Computational Study, *J. Phys. Chem. A*, 2016, **120**(39), 7659–7670.

52 M. Primet, J. C. Vedrine and C. Naccache, Formation of rhodium carbonyl complexes in zeolite, *J. Mol. Catal.*, 1978, **4**(6), 411–421.

53 L. Liu and A. Corma, Metal Catalysts for Heterogeneous Catalysis: From Single Atoms to Nanoclusters and Nanoparticles, *Chem. Rev.*, 2018, **118**(10), 4981–5079.

